THE JOURNAL OF BIOLOGICAL CHEMISTRY VOL. 291, NO. 34, pp. 17569–17578, August 19, 2016

The Cataract-linked Mutant Connexin50D47A Causes Endoplasmic Reticulum Stress in Mouse Lenses*[S]

Received for publication, December 1, 2015, and in revised form, June 14, 2016 Published, JBC Papers in Press, June 17, 2016, DOI 10.1074/jbc.M115.707950

Viviana M. Berthoud[‡1], Peter J. Minogue[‡], Paul A. Lambert[§], Joseph I. Snabb[‡], and Eric C. Beyer[‡]

From the [‡]Department of Pediatrics and the [§]Pritzker School of Medicine, University of Chicago, Chicago, Illinois 60637

Mice expressing connexin50D47A (Cx50D47A) exhibit nuclear cataracts and impaired differentiation. Cx50D47A does not traffic properly, and homozygous mutant lenses show increased levels of the stress-responsive αB-crystallins. Therefore, we assessed whether expression of Cx50D47A led to endoplasmic reticulum (ER) stress in the lens *in vivo*. Although pharmacologic induction of ER stress can be transduced by three different pathways, we found no evidence for activation of the IRE1α or ATF6 pathways in Cx50D47A-expressing lenses. In contrast, heterozygous and homozygous Cx50D47A lenses showed an increase in phosphorylated PERK immunoreactivity and in the ratio of phosphorylated to total EIF2α (2.4- and 3.3-fold, respectively) compared with wild type. Levels of ATF4 were similar in wild type and heterozygous lenses but elevated in homozygotes (391%). In both heterozygotes and homozygotes, levels of calreticulin protein were increased (184 and 262%, respectively), as was *Chop* mRNA (1.9- and 12.4-fold, respectively). CHOP protein was increased in homozygotes (384%). TUNEL staining was increased in Cx50D47A lenses, especially in homozygous mice. Levels of two factors that may be pro-survival, *Irs2* and *Trib3*, were greatly increased in homozygous lenses. These results suggest that expression of Cx50D47A induces ER stress, triggering activation of the PERK-ATF4 pathway, which potentially contributes to the lens pathology and leads to increased expression of anti-apoptotic factors, allowing cell survival.

Proteins that do not traffic properly or are misfolded can cause endoplasmic reticulum (ER)[2] stress. To compensate for the disturbance of proteostasis, cells transduce ER stress through at least three different signaling pathways: (*a*) the inositol-requiring enzyme 1 (IRE1α)-dependent, (*b*) the activating transcription factor 6 (ATF6)-dependent, and (*c*) the PRKR-like ER kinase (PERK)-dependent pathways. Prolonged and uncompensated ER stress triggers the unfolded protein response (UPR), which may ultimately target the cells for apoptosis.

Many disease-linked connexin mutants show impaired cellular trafficking. One such mutant has a missense mutation in the lens gap junction protein, connexin50 (Cx50), affecting amino acid residue 47 (Cx50D47N in humans and Cx50D47A in mice) and is linked to congenital cataracts (1, 2). When expressed in transfected cells, Cx50D47N and Cx50D47A localize mostly within the ER (1). Lenses from mice expressing Cx50D47A have nuclear cataracts, reduced sizes, and impaired denucleation (3). Some immunoreactive Cx50 localizes intracellularly in lens epithelial cells from these mice (3). Homozygous Cx50D47A lenses have increased levels of αB-crystallins (3), which are responsive to several types of stress in different cell types, including lens epithelial cells (4–7). These observations suggest that expression of a Cx50D47 mutant may cause ER stress in the lens and contribute to pathology in this organ.

The current understanding of cellular responses to ER stress is based on many studies in cultured cells and fewer studies *in vivo*. Although massive induction of ER stress by pharmacological agents may activate all three transducing pathways, the UPR is a regulated pathway that may differentially use the transducing pathways, depending on the stimulus causing the ER stress. To elucidate the effects of *in vivo* expression of a connexin with impaired trafficking, we studied the Cx50D47A mouse and examined the activation of each of the ER stress-transducing signaling pathways in the lens. We found evidence for activation of the PERK-dependent pathway, but not of the IRE1α- or ATF6-dependent pathways, in Cx50D47A-expressing lenses.

Results

The Ire1α-dependent Pathway Is Not Activated in 1-Month-old Cx50D47A Mice—Activation of the IRE1α pathway leads to splicing of its downstream target, *Xbp-1* (X-box-binding protein 1) RNA. To test whether this ER stress-transducing pathway was activated in Cx50D47A-expressing lenses, we determined the relative levels of spliced *Xbp-1* transcripts on the lens by RT-qPCR. Although variations in the levels of spliced *Xbp-1* transcripts were detected among individuals (even within each genotype), they correlated with proportional changes in mRNA levels for total *Xbp-1*. Indeed, the spliced/total ratios of *Xbp-1* transcripts in samples from heterozygous and homozygous animals were similar to those in wild type mice (Fig. 1), suggesting that this pathway is not activated by expression of Cx50D47A. As a positive control, a wild type lens was treated with thapsigargin, a non-competitive inhibitor of the sarcoendoplasmic reticulum calcium transport ATPase (SERCA), which induces the UPR pharmacologically. The

* This work was supported by National Institutes of Health Grant RO1EY08368 (to E. C. B.) and NIDDK Grant 2T35DK062719 (to P. A. L. as a trainee). The authors declare that they have no conflicts of interest with the contents of this article. The content is solely the responsibility of the authors and does not necessarily represent the official views of the National Institutes of Health.

[S] This article contains supplemental Fig. 1.

[1] To whom correspondence should be addressed: Dept. of Pediatrics, University of Chicago, KCBD-5, 900 E. 57th St., Chicago, IL 60637. Tel.: 773-834-2115; Fax: 773-834-1329; E-mail: vberthou@peds.bsd.uchicago.edu.

[2] The abbreviations used are: ER, endoplasmic reticulum; CHOP, C/EBP-homologous protein; Cx, connexin; UPR, unfolded protein response; RT-qPCR, reverse transcription-quantitative PCR.

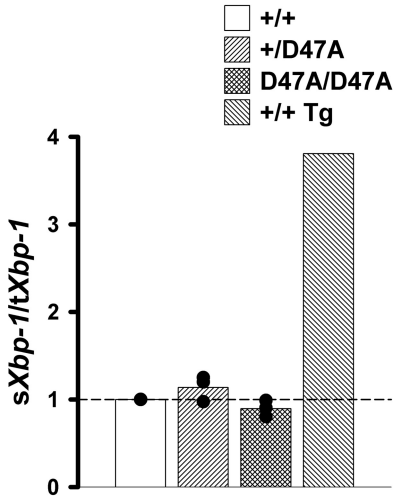

FIGURE 1. **Expression of Cx50D47A does not activate the IRE1α-dependent pathway.** The graph shows the ratio of spliced (s*Xbp-1*) over total (t*Xbp-1*) *Xbp-1*-fold changes for 1-month-old Cx50D47A heterozygous (+/D47A) and homozygous (D47A/D47A) lenses relative to wild type (+/+) littermates as determined by RT-qPCR obtained in three independent experiments (*black circles*). The *bars* represent the arithmetic means of the ratios for each genotype. The *short dashed line* marks the reference value of wild type mice (s*Xbp-1*/t*Xbp-1* = 1.0). A thapsigargin-treated wild type lens (+/+ *Tg*) was used as a positive control; the change in its s*Xbp-1*/t*Xbp-1* ratio is shown on the *right*.

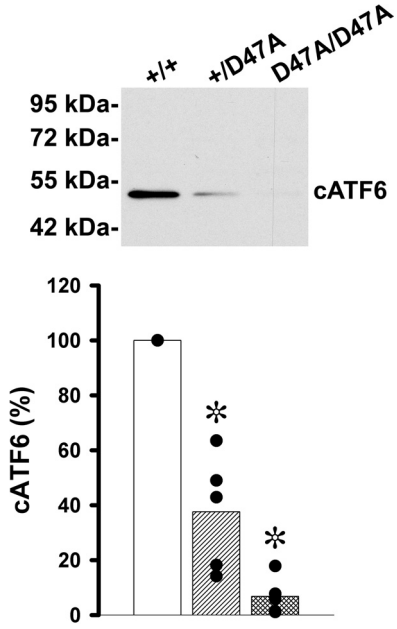

FIGURE 2. **Levels of ATF6 are decreased in Cx50D47A mice.** Shown is an immunoblot of ATF6 in whole lens homogenates from 1-month-old wild type (+/+), heterozygous (+/D47A), and homozygous (D47A/D47A) mice after loading 100 μg of total protein in each lane. The migration positions of the molecular mass markers are indicated on the *left*. The graph shows the quantification of the immunoreactive band obtained in five independent experiments (*black circles*). The *bars* represent the averages of the values obtained for each genotype. Significant differences between wild type and heterozygous or wild type and homozygous Cx50D47A lenses are indicated by *asterisks* ($p < 0.05$).

spliced/total ratio of *Xbp-1* transcripts in this sample was 3.8 (Fig. 1).

The ATF6α-dependent Pathway Is Not Activated in Cx50D47A Mice—ER stress-induced activation of the ATF6 pathway leads to translocation of ATF6α from the ER to the Golgi compartment, where it is cleaved by SP1 and SP2 (8), resulting in a change in apparent molecular mass from 90 to 50 kDa (9). To test whether expression of Cx50D47A led to activation of the ATF6-dependent transducing pathway, whole lens homogenates were subjected to immunoblotting with anti-ATF6α antibodies. Although the antibody recognizes both the full-length and cleaved forms of ATF6α, only the cleaved form was detected in lens samples (Fig. 2). Surprisingly, levels of cleaved ATF6α were significantly decreased in both heterozygous and homozygous Cx50D47A mice, respectively, representing on average 37.6 and 6.8% of the values detected in wild type littermates (Fig. 2), suggesting deactivation of this pathway in the mutant mice.

The PERK-dependent Pathway Is Activated by Expression of Cx50D47A—Activation of the PERK-dependent signaling pathway involves PERK autophosphorylation. To test whether Cx50D47A led to activation of this pathway, we performed immunofluorescence on lens sections using an antibody that specifically detects the active (phosphorylated) form of PERK (P-PERK). Most of the P-PERK immunoreactivity appeared as small puncta located in epithelial and fiber cells near the bow region (Fig. 3, *A–F*). A significant increase in immunoreactive P-PERK was detected in sections from heterozygous and homozygous Cx50D47A mice as compared with wild type animals (Fig. 3*G*), but the increase did not reach statistical significance between heterozygous and homozygous lenses. Because activation of PERK leads to phosphorylation of EIF2α, we performed immunoblots to determine whether it occurred in Cx50D47A-expressing lenses. Heterozygous lenses showed a significant 1.4-fold increase in the relative ratio of phosphorylated to total EIF2α (P-EIF2α/EIF2α) above the ratio in wild type lenses, and homozygous lenses showed a significant 2.3-fold increase over the wild type ratio (Fig. 3*H*). Because phosphorylation of EIF2α may lead to increased translation of ATF4 (activating transcription factor 4 (CREB2)), we determined its levels in the lens. Levels of ATF4 were significantly increased in lenses from homozygous Cx50D47A mice, representing on average 391% of the levels detected in wild type mice, whereas levels of ATF4 in heterozygous lenses were similar to those of wild type animals (Fig. 3*I*).

To test whether expression of Cx50D47A altered transcription or levels of ER proteins, we performed RT-qPCR and immunoblotting. Protein levels of the calcium-binding chaperone, calreticulin, which is mainly localized in the ER, were significantly increased in Cx50D47A-expressing lenses; they represented on average 184% in heterozygous and 262% in homozygous lenses of the calreticulin levels in wild type littermates (Fig. 4*A*). Levels of GRP78 (also known as BIP) were significantly increased in heterozygous and homozygous lenses (146 and 164%, respectively) relative to the levels in wild type lenses (Fig. 4*B*). The mRNA levels for two other ER-resident proteins that are often increased in the UPR, *p58^{IPK}* (a co-chaperone of heat shock 70-kDa protein 8) and *Erp72* (a protein-disulfide isomerase), were similar among all genotypes (Fig. 4, *C* and *D*).

In the canonical ER stress response, increased transcription of CHOP is downstream from ATF4. To test whether the

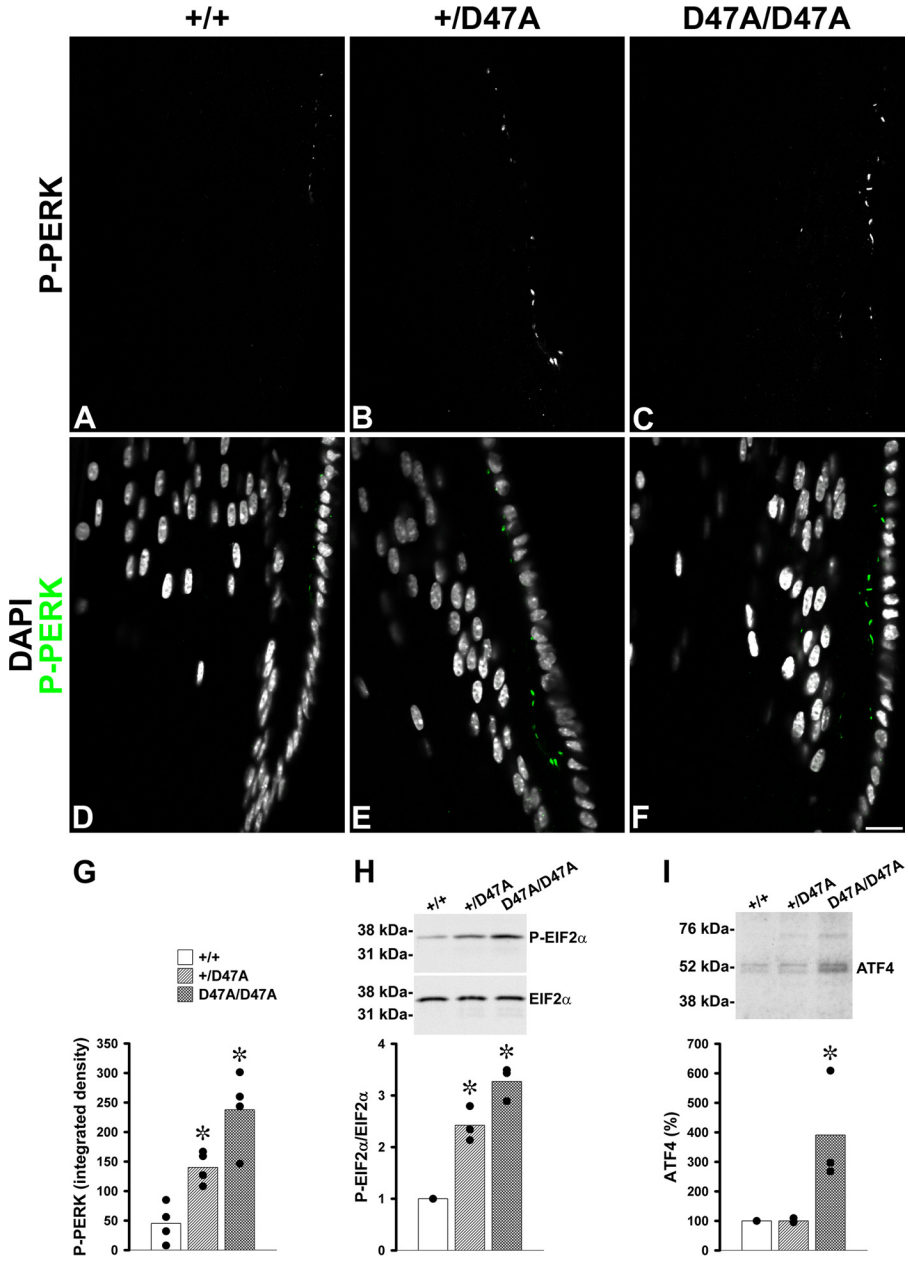

FIGURE 3. **The PERK-dependent pathway is activated in Cx50D47A mice.** *A–F*, confocal images show immunoreactive P-PERK (*A–C*) and its overlap with DAPI staining (*D–F*; P-PERK immunoreactivity in *green* and DAPI staining in *gray*/*white*) in the bow region of longitudinal sections from lenses of 1-month-old wild type (+/+) (*A* and *D*), heterozygous (+/D47A) (*B* and *E*), and homozygous (D47A/D47A) (*C* and *F*) animals. *Bar*, 18.4 μm. *G*, graph illustrating the quantification of P-PERK immunoreactive particles presented as the integrated density in arbitrary units ($n = 4$). *H*, immunoblots of immunoreactive phosphorylated (*top*) and total (*bottom*) EIF2α in total lens homogenates from 1-month-old wild type (+/+) and Cx50D47A heterozygous (+/D47A) and homozygous (D47A/D47A) mice. Fifteen μg of total protein were loaded in each lane to detect phosphorylated EIF2α; 60 μg of total protein were loaded per lane to detect total EIF2α. The migration positions of the molecular mass markers are indicated on the *left*. The densitometric values of the bands obtained in three independent experiments were used to calculate the phosphorylated/total EIF2α ratios (P-EIF2α/EIF2α). The graph shows the P-EIF2α/EIF2α relative to the value obtained in wild type littermates (*black circles*). *I*, immunoblot of immunoreactive ATF4 in aliquots of total lens homogenates from 1-month-old wild type (+/+), and Cx50D47A heterozygous (+/D47A) and homozygous (D47A/D47A) mice containing 100 μg of total protein. The migration positions of the molecular mass markers are indicated on the *left*. The graph shows the densitometric values of the bands obtained in three independent experiments expressed as percentages of the values obtained in wild type animals (*black circles*). The *bars* in *G–I* indicate the average value for each genotype. *Asterisks* denote significant differences from wild type values ($p < 0.05$).

increased levels of ATF4 resulted in alterations in CHOP, we determined its transcript and protein levels. We detected significant increases of *Chop* mRNA in heterozygous and homozygous lenses (1.9- and 12.4-fold on average, respectively) compared with the levels detected in wild type lenses (Fig. 5*A*). A CHOP-immunoreactive band was clearly visible in immunoblots of samples from Cx50D47A homozygous mice, but this band was only barely detectable in heterozygous and wild type samples, implying that overall levels of the CHOP protein are extremely low in the normal lens (Fig. 5*B*). Levels of CHOP in homozygotes represented on average 384% of wild type levels ($p < 0.05$), whereas CHOP levels in heterozygotes were on average 73% of wild type levels ($p = 0.3$). To determine the cellular compartment of CHOP localization, we performed immuno-

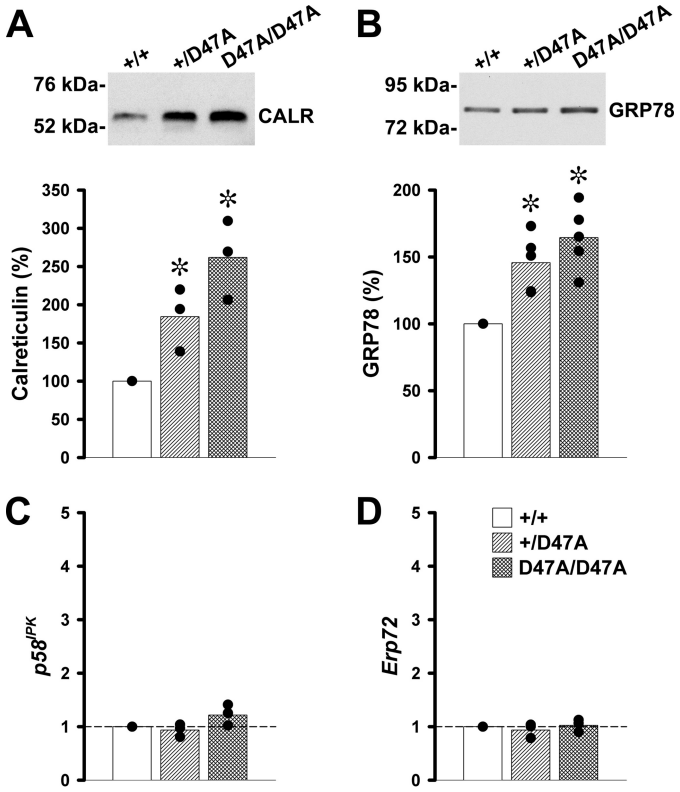

FIGURE 4. **Levels of lens calreticulin and GRP78 are increased in Cx50D47A-expressing mice.** *A* and *B*, immunoblots of calreticulin (CALR) and GRP78 in whole lens homogenates from 1-month-old wild type (+/+) and Cx50D47A heterozygous (+/D47A) and homozygous (D47A/D47A) mice. Each *lane* was loaded with 60 μg of total protein to detect calreticulin or with 20 μg of total protein to detect GRP78. The migration positions of the molecular mass markers are indicated on the *left*. The graphs show the quantification of the immunoreactive bands obtained in independent experiments expressed as a percentage of the values obtained in wild type littermates (*black circles*) ($n = 3$ for CALR and $n = 5$ for GRP78). The *bars* represent the average of the values obtained. *Asterisks* indicate a significant difference from wild type values ($p < 0.05$). *C* and *D*, graphs show the -fold change of $p58^{IPK}$ and *Erp72* transcript levels in 1-month-old Cx50D47A heterozygous (+/D47A) and homozygous (D47A/D47A) lenses relative to wild type (+/+) littermates as determined by RT-qPCR. The *bars* represent the geometric mean of the values obtained in three independent experiments (*black circles*). The *dashed line* marks the value of wild type mice (1.0).

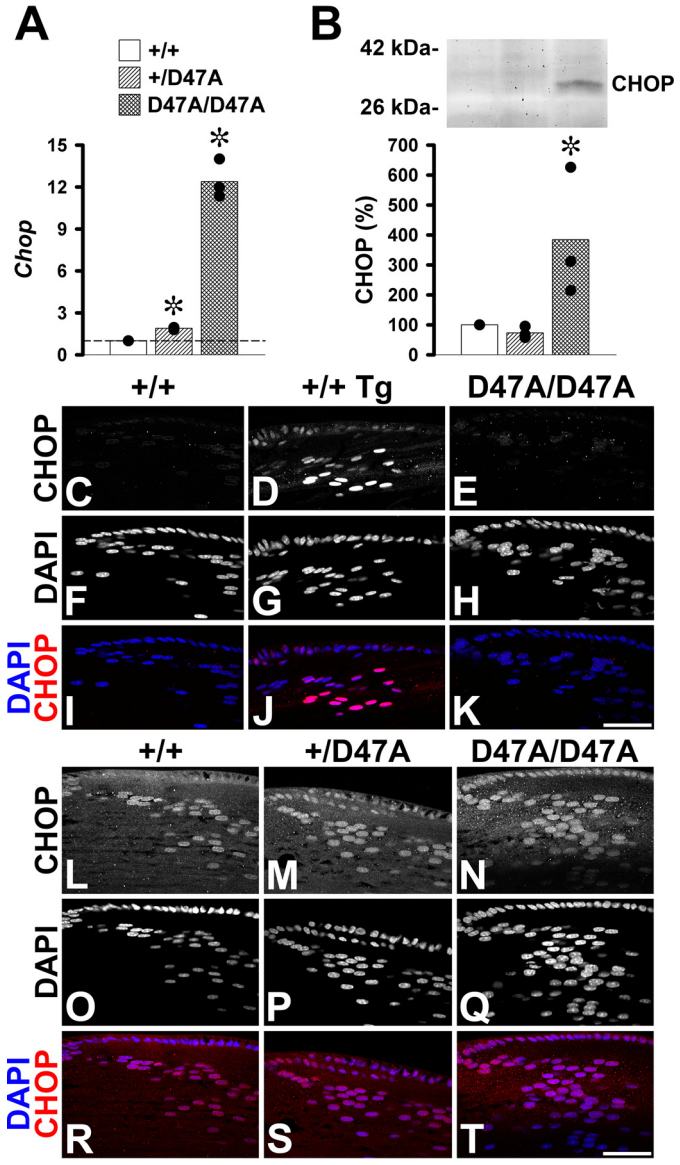

FIGURE 5. **Expression of Cx50D47A increases levels of CHOP.** *A*, graph shows the -fold change on transcript levels for *Chop* in 1-month-old Cx50D47A heterozygous (+/D47A) and homozygous (D47A/D47A) lenses relative to wild type littermate lenses (+/+) as determined by RT-qPCR. The values obtained in each of three independent experiments are shown in *black circles*. The *bars* represent the geometric mean of the -fold change obtained in the individual experiments. The value obtained in wild type mice was considered as the reference (*short dashed line* at *Chop* = 1). *B*, immunoblot of CHOP in aliquots of total homogenates from lenses of 1-month-old wild type mouse (+/+) and Cx50D47A heterozygous (+/D47A) and homozygous (D47A/D47A) littermates containing 120 μg of total protein. The migration positions of the molecular mass markers are indicated on the *left*. The graph shows the mean (*bar*) of the densitometric values obtained in three independent experiments (*black circles*) expressed as percentages of the values obtained in wild type lenses. *Asterisks* denote significant differences from wild type values ($p < 0.05$). *C–K*, confocal images show the distribution of CHOP (*C–E*), DAPI staining (*F–H*), and the overlap of the CHOP (*red*) and DAPI (*blue*) fluorescent signals (*I–K*) in the bow region of longitudinal sections from 1-month-old untreated wild type (+/+) (*C*, *F*, and *I*), thapsigargin-treated wild type (+/+ Tg) (*D*, *G*, and *J*), and untreated homozygous (D47A/D47A) (*E*, *H*, and *K*) lenses acquired at optimized settings for photographing the thapsigargin-treated lens. *L–T*, confocal images show the distribution of CHOP (*L–N*), DAPI staining (*O–Q*), and the overlap of the CHOP (*red*) and DAPI (*blue*) signals (*R–T*) in the bow region of longitudinal sections from 1-month-old wild type (+/+) (*L*, *O*, and *R*), heterozygous (+/D47A) (*M*, *P*, and *S*), and homozygous (D47A/D47A) (*N*, *Q*, and *T*) lenses at optimized settings for photographing untreated lenses. *Bar*, 49.1 μm.

fluorescence. Immunoreactive CHOP staining was localized to nuclei of cells in the epithelium and bow region of all genotypes and in wild type lenses treated with thapsigargin *in vitro* to induce UPR (Fig. 5, *C–T*). Lenses from wild type (Fig. 5, *C*, *F*, and *I*) or Cx50D47A homozygous (Fig. 5, *E*, *H*, and *K*) mice showed much weaker CHOP immunoreactivity than wild type lenses treated with thapsigargin (Fig. 5, *D*, *G*, and *J*), suggesting that the endogenous ER stress induced by expression of Cx50D47A is milder than an abrupt pharmacologically induced ER stress.

Because increased CHOP can lead to apoptosis, we performed TUNEL staining on lens sections. In 1-month-old wild type lenses, fluorescent puncta were detected within a few cells at the border of the organelle-free zone (where they often co-localized with DAPI-stained material probably representing cells undergoing denucleation, which is part of the normal process of fiber cell differentiation), as expected from previous studies of normal lenses (10). Less frequently, fluorescent puncta (that did not co-localize with DAPI-stained material)

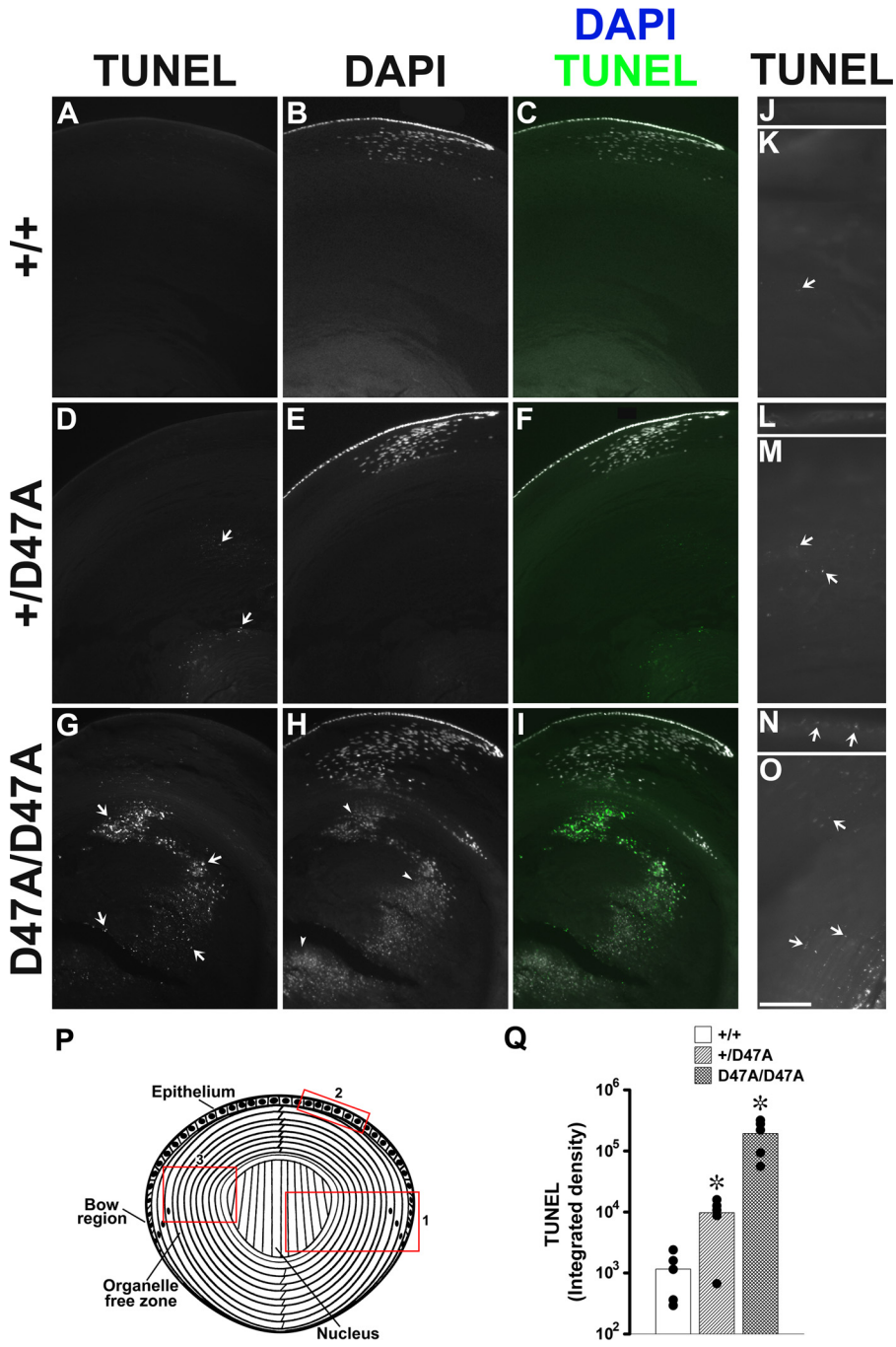

FIGURE 6. **TUNEL staining is increased in Cx50D47A lenses.** *A–I*, photomicrographs show the distribution of TUNEL staining (*TUNEL*) (*A*, *D*, and *G*), DAPI staining (*B*, *E*, and *H*), and their overlap (*C*, *F*, and *I*; TUNEL in *green*, DAPI in *gray/white*) on longitudinal sections from 1-month-old wild type (+/+) (*A–C*) and Cx50D47A heterozygous (+/D47A) (*D–F*) and homozygous (D47A/D47A) (*G–I*) lenses at low power magnification. *Arrows* point to TUNEL-positive staining in *D* and *G*, and *arrowheads* point to nuclear remnants in *H*. *J–O*, photomicrographs show TUNEL staining of epithelium (*J*, *L*, and *N*) and the region encompassing the cortical fibers between the epithelium and the periphery of the lens nucleus (*K*, *M*, and *O*) on longitudinal sections from 1-month-old wild type (+/+) (*J* and *K*), heterozygous (+/D47A) (*L* and *M*), and homozygous (D47A/D47A) (*N* and *O*) lenses. *Bar*, 158.5 μm (*A–I*), 135.4 μm (*J*), 78.4 μm (*K*), 105.1 μm (*L*), 87.2 μm (*M*), 68.3 μm (*N*), and 97.5 μm (*O*). *P*, diagram of the lens to illustrate the areas corresponding to the images shown in *A–I* (*red box 1*); *J*, *L*, and *N* (*red box 2*); and *K*, *M*, and *O* (*red box 3*). *Q*, graph shows the quantification of TUNEL staining (logarithmic scale) as integrated density for wild type (+/+) and Cx50D47A heterozygous (+/D47A) and homozygous (D47A/D47A) lenses in five independent experiments (*black circles*). The *bars* show the average value for all experiments. *Asterisks* denote a significant difference as compared with wild type animals ($p < 0.05$).

were detected in cells within the organelle-free zone (Fig. 6, *A–C*, *J*, and *K*). In contrast, within homozygous Cx50D47A lens sections, many TUNEL-stained puncta were detected that co-localized with some nuclei and many nuclear remnants (*i.e.* DAPI-stained material of smaller size and different morphology than the intact nuclei in epithelia and early differentiating fiber cells), most of which localized toward the center of the lens (Fig. 6, *G–I*). Sections from Cx50D47A heterozygous lenses also showed an increase in TUNEL-stained puncta compared with wild type lenses but less than that seen in homozygotes (Fig. 6, *D–F*). Examination of these samples at higher magnification revealed low intensity TUNEL-fluorescent puncta in the

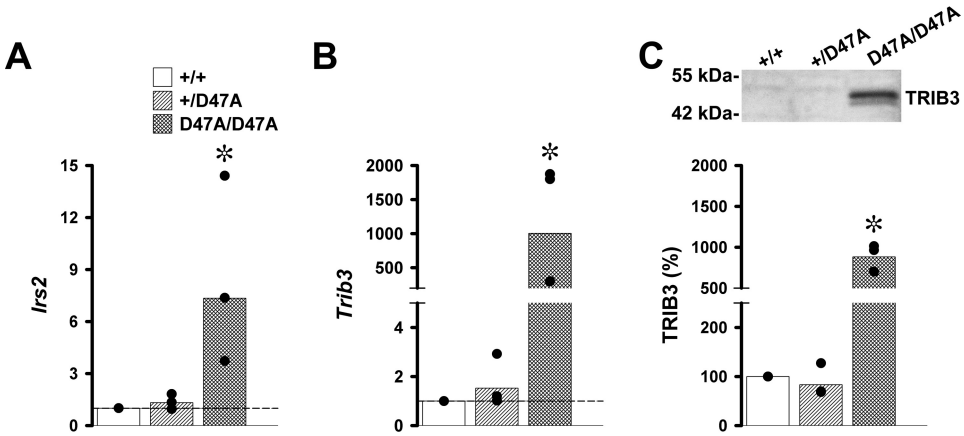

FIGURE 7. ***Irs2* and *Trib3* are increased in homozygous Cx50D47A lenses.** *A* and *B*, graphs show the -fold increase in *Irs2* and *Trib3* mRNAs in 1-month-old Cx50D47A heterozygous (+/D47A) and homozygous (D47A/D47A) lenses relative to the values of wild type (+/+) littermates (*short-dashed line* at *1*) obtained in three independent experiments (*black circles*). The *bars* represent the geometric means of the -fold change obtained in the individual experiments. *C*, immunoblot of TRIB3 in lens samples from 1-month-old wild type (+/+) and Cx50D47A heterozygous (+/D47A) and homozygous (D47A/D47A) mice containing 140 μg of total protein. The migration positions of the molecular mass standards are shown on the *left*. The graph shows the average densitometric value (*bar*) of the TRIB3 bands in three independent experiments (*black circles*). *Asterisks* indicate a significant difference as compared with wild type animals ($p < 0.05$).

epithelia and differentiating fiber cells from Cx50D47A heterozygous and homozygous lenses that were seldom detected in wild type lenses (Fig. 6, *J–O*). Quantitative analyses of integrated density revealed a significant increase in TUNEL staining in heterozygous and homozygous samples compared with wild type (Fig. 6*Q*). When considered as ratios, the integrated densities of TUNEL staining were 19.6 times (heterozygotes) and 371 times (homozygotes) that of the wild type.

These results presented a conundrum. Activation of the PERK-dependent UPR pathway (with increase in ATF4 and CHOP levels) in Cx50D47A homozygotes should have resulted in severe apoptosis and cell death. However, not all lens cells showed signs of DNA fragmentation after TUNEL staining. This prompted us to look for factors that might increase cell survival. Transcripts for *Trib3* (Tribbles pseudokinase 3) and *Irs2* (insulin receptor substrate 2) have been identified as pro-survival genes in early stage erythroblasts (which lose their nuclei during differentiation like lens cells) (11). To test whether expression of Cx50D47A increased levels of *Trib3* and *Irs2* transcripts, we performed RT-qPCR. Levels of both *Trib3* and *Irs2* were significantly increased in Cx50D47A homozygotes, whereas the values in heterozygotes were similar to those in wild type animals (Fig. 7, *A* and *B*). The increase was, on average, 1.3-fold in heterozygotes and 7.3-fold in homozygotes for *Irs2* and 1.5- and 1000-fold for *Trib3*. Because *Trib3* transcription is a direct target of CHOP, and TRIB3 inhibits the transcriptional activity of ATF4 and CHOP, we used immunoblotting to determine whether the levels of TRIB3 were increased. A TRIB3-immunoreactive band was detected in samples from Cx50D47A homozygous lenses, whereas TRIB3 was almost undetectable in samples from wild type and Cx50D47A heterozygous lenses (Fig. 7*C*). On average, levels of TRIB3 protein represented 83% (heterozygotes) and 881% (homozygotes) of the values in wild type lenses (Fig. 7*C*).

Discussion

Cx50D47A does not traffic properly and is retained intracellularly, mostly in the endoplasmic reticulum (1). In this study, we have shown that expression of this mutant induced ER stress in the lenses of both heterozygous and homozygous mutant mice. The induced ER stress was transduced through the PERK-dependent pathway. The extent of activation of this pathway was more pronounced in homozygotes than in heterozygotes. We did not detect activation of the other two signal transduction pathways; the degree of activation of the Ire1α pathway was unchanged, whereas the ATF6 pathway was significantly decreased.

A common characteristic of ER stress is the expansion of the endoplasmic reticulum. Such an expansion may be responsible for the 84 and 162% increases in calreticulin levels in heterozygous and homozygous Cx50D47A lenses. This may result from an increase in the capacity of the ER per cell or from an increase in the number of lens cells containing ER, because Cx50D47A lenses have organelle-containing cells reaching farther into the organ than do wild type lenses (3). The expansion did not increase all ER-resident proteins to the same extent. GRP78 levels increased by about 50% in both heterozygous and homozygous lenses. Protein-disulfide isomerase increased by about 13% in heterozygous and 21% in homozygous lenses (3). Moreover, the transcript levels for other ER-resident proteins (*i.e.* $p58^{IPK}$ and ERP72) were unchanged. These results imply that expression of Cx50D47A caused expansion of the ER with selective changes among ER-resident proteins, as has been observed after induction of ER stress in other cell types (12, 13).

The canonical ER stress-induced PERK signaling pathway is characterized by elevated phosphorylation of PERK, which increases phosphorylation of EIF2α. Phosphorylation of EIF2α results in inhibition of general protein translation (14) and selective translation of ER chaperones and the transcription factor ATF4. ATF4 in turn increases transcription of several proteins, including the transcription factor CHOP (Fig. 8). In Cx50D47A mice, P-PERK immunostaining in heterozygous and homozygous lenses was significantly higher than in wild type lenses, suggesting activation of this ER stress signaling pathway. Although the increase in P-PERK immunostaining

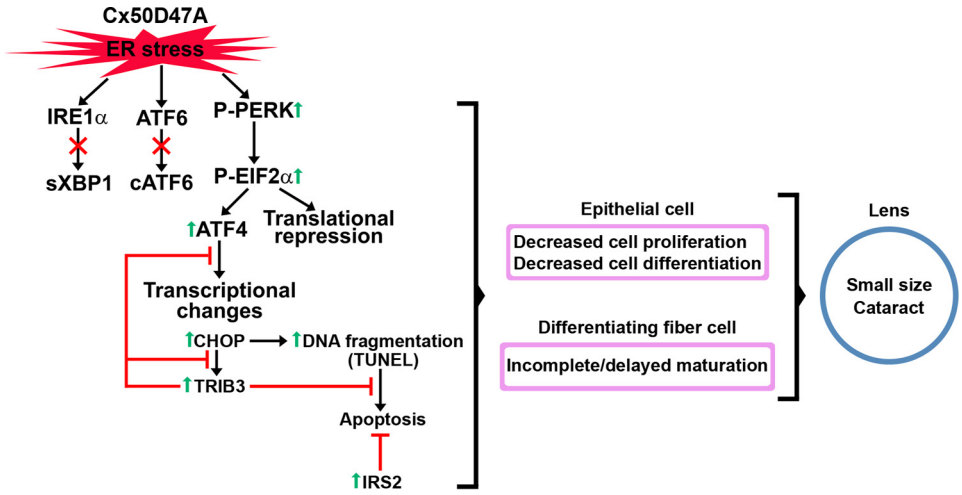

FIGURE 8. **Mechanism implicated in the phenotype of Cx50D47A lenses.** The diagram illustrates the mechanism by which Cx50D47A induces ER stress, leading to activation (phosphorylation) of PERK. P-PERK phosphorylates EIF2α, which leads to general translational repression and to increased selective protein translation, including calreticulin and the transcription factor ATF4. ATF4 increases transcription of *Chop*, which leads to increased DNA fragmentation (TUNEL), and some lens cells may undergo apoptosis. CHOP increases *Trib3* transcripts, and the TRIB3 protein inhibits the transcriptional activity of ATF4 and CHOP. The increase in TRIB3 and IRS2 allows survival of lens cells. The ER stress and attenuation of general protein translation contribute to decreased proliferation and differentiation of epithelial cells and incomplete/delayed fiber cell maturation. These changes contribute to small lenses with cataracts in Cx50D47A mice.

did not reach statistical significance between Cx50D47A heterozygotes and homozygotes, downstream targets exhibited differences suggesting that their activation was greater in homozygotes. Heterozygous Cx50D47A lenses showed smaller increases of the P-EIF2α/EIF2α ratio and of *Chop* transcripts than homozygous Cx50D47A lenses and showed no increases of CHOP or ATF4 protein levels. Homozygous Cx50D47A lenses showed a significant increase in ATF4 levels associated with increases in *Chop* transcript and protein, suggesting activation of a UPR. These changes probably occurred in organelle-containing fiber cells that reach deeper into the lens in Cx50D47A mice (3).

Persistent activation of PERK signaling (as occurs in Cx50D47A lenses) has been associated with impaired cell proliferation and a global decrease in protein synthesis (15). Decreased cell proliferation and inhibition of general protein synthesis probably contribute to the decrease in lens size observed in heterozygous and homozygous Cx50D47A mice (3). The decrease in general protein translation may partially explain the severe reductions (>80%) in Cx50 levels in these mutant mice, but it cannot fully explain the decrease, because levels of other proteins (including Cx46) did not decrease to the same extent (3). Levels of selected proteins might be reduced by degradation through the ubiquitin-proteasome system or autophagy; ER stress or the UPR can interface with these pathways to preserve proteostasis (16). Thus, both inhibition of general protein synthesis and activation of selective protein degradation may contribute to the incomplete differentiation of fiber cells in Cx50D47A mice. Similarly, incomplete differentiation was observed in C2C12 myoblasts overexpressing the spliced form of *Xbp1*, since they did not generate mature myotubes when induced to differentiate (17).

Elevated PERK signaling can increase either cell survival or apoptosis, depending on the differential activation of downstream targets (15, 18). Homozygous Cx50D47A lenses showed aspects of both kinds of responses. They exhibited increases in *Chop* transcripts and CHOP protein, which are most commonly associated with apoptosis. TUNEL staining (which detects DNA strand breaks) was increased and was most evident toward the center of the lens. Some epithelial or differentiating fiber cells may have undergone apoptosis, contributing to the smaller lens size. However, homozygous Cx50D47A lenses also showed increased levels of *Trib3* and *Irs2* transcripts, both of which have been identified as pro-survival factors in early stage erythroblasts when erythropoietin is limiting (11). *Trib3* is a downstream target of CHOP and can inhibit the transcriptional activities of ATF4 and CHOP (19, 20). TRIB3 has been ascribed pro-apoptotic effects in other systems. Thus, it may act as a switch between survival and apoptosis, with its pro- or anti-apoptotic function depending on cell type, context, and extent of activation. The ability of TRIB3 to regulate its own expression by inhibiting the transcriptional activity of ATF4 suggests that the fates of different cells may depend on the levels of TRIB3 protein attained in each cell. In the lens, TRIB3 (in combination with IRS2) may have acted as a pro-survival factor, because these lenses are already compromised due to the decrease in connexin levels, which would limit intercellular transfer of nutrients and signaling molecules to the center of the lens. Thus, the activities of IRS2 and TRIB3 acting as pro-survival factors may explain the lack of massive TUNEL staining in differentiating fibers (as would be expected from the increase in CHOP) and the absence of remarkable findings in hematoxylin- and eosin-stained Cx50D47A lens sections (2). ATF4 has previously been implicated in lens cell survival, because lenses from ATF4 knock-out mice undergo apoptotic cell death and ultimately degenerate (21). Thus, the consistent increase in ATF4 levels that we observed in 1-month-old homozygous Cx50D47A lenses may correspond to a compensatory change to avoid apoptotic cell death.

Our results obtained from Cx50D47A mice suggest that other connexin mutants may also contribute to pathology through ER stress and the UPR. Lenses of 2-month-old mice

heterozygous for Cx50G22R or Cx50S50P contain increased levels of spliced *Xbp-1* transcripts (without corresponding changes in protein), suggesting that the IRE1α-dependent pathway may be activated (22). However, these results contrast with our observations that the IRE1α-dependent pathway was not activated in Cx50D47A lenses; rather, the PERK-dependent pathway was stimulated. This implies that the ER stress induced by diverse Cx50 mutants may be transduced through different signaling pathways. ER stress-induced cell death through activation of the UPR has been reported for mammalian cells transfected with skin disease-linked Cx31 mutants (23); however, it remains to be determined whether ER stress contributes to the phenotype of connexin mutant-linked diseases other than cataracts *in vivo*.

ER stress and the UPR may have roles in cataracts caused by different etiologies. Previous studies have reported that ER stressors activate the UPR in lens epithelial cells, leading to increased levels of GRP78 (BIP) and ATF4 (24). Additionally, lens epithelial cells from galactosemic rats show increased levels of ATF4, GRP78, CHOP, and cell death (25). In these studies, the relative increase in levels of GRP78 was more pronounced than that of ATF4, whereas the opposite was true in Cx50D47A homozygous lenses. Similar to our data on Cx50D47A mice, an increase in ATF4 levels associated with a decrease in ATF6 levels was observed in homozygous αA-R49C-crystallin knock-in lenses (26). However, the homozygous αA crystallin mutant lenses show more severe changes than the Cx50D47A lenses, including a 5-fold increase in GRP78 levels, vacuoles, highly disorganized fiber cells, and increased epithelial and fiber cell death (26, 27). The different magnitude of increase in GRP78 levels in this mouse model compared with Cx50D47A mice may be due to the different roles of Cx50 and of α-crystallins (which act as molecular chaperones) (28). Thus, the transducing pathways and the extent of activation of ER stress and UPR differ in cataracts of different etiologies. Moreover, the Cx50D47A mouse lenses have substantial compensatory mechanisms allowing cell survival and amelioration of cataract development.

Activation of UPR components contributes to differentiation programs of various cells, including those in the lens (29). Activation of the PERK-dependent pathway may contribute to decreased cell proliferation and differentiation of epithelial cells and to incomplete (or delayed) maturation of differentiating fiber cells. The severe reduction of Cx50 levels probably also contributes to the small lenses in Cx50D47A mice, because deletion of Cx50 (in Cx50-null homozygotes) results in decreased lens size (30, 31) ascribed to reduced cell proliferation (32). Thus, activation of the PERK-dependent pathway together with Cx50 deficiency in the Cx50D47A mice may produce a more severe phenotype compared with that in Cx50-null mice (*i.e.* smaller lenses with nuclear cataracts in both Cx50D47A heterozygotes and homozygotes) (Fig. 8). Our results imply that expression of Cx50D47A disturbs the normal and controlled (*i.e.* constitutive) UPR activation, inducing a more persistent ER stress. We propose that a novel state of adaptation allows lens cell survival in the mutant mouse lenses.

Experimental Procedures

Chemicals—All chemicals were obtained from Sigma or Fisher unless otherwise specified.

Antibodies—Rabbit polyclonal anti-ATF6 antibodies (3683; lot 7253-1203) were obtained from ProSci Inc. (Poway, CA). Rabbit polyclonal anti-ATF4(Creb-2) (sc-200; lot L3113) and mouse monoclonal anti-CHOP/GADD 153 (B3) (sc-7351; lot D0815) antibodies were obtained from Santa Cruz Biotechnology, Inc. (Dallas, TX). Rabbit polyclonal anti-GRP78/BiP (ab21685; GR219186-1) antibodies were obtained from Abcam (Cambridge, MA). Rabbit monoclonal anti-EIF2α (D7D3) (5324P; lot 3), anti-P-EIF2α (Ser-51) (D9G8) (3398P; lot 2), anti-P-PERK (Thr-980) (16F8) (3179S; lot 13), and anti-calreticulin (DE36) (12238P; lot 1) antibodies were obtained from Cell Signaling Technology (Danvers, MA). Mouse monoclonal anti-CHOP (9C8) antibody (MA1-250; lot QJ222637) was obtained from Thermo Fisher Scientific. Rabbit polyclonal anti-TRIB3(1–145) antibodies (ST1032; lot 2655006) were obtained from EMD Millipore (Billerica, MA). Alexa Fluor® 488 goat anti-rabbit IgG (A-11034; lot 1705912) and Alexa Fluor® 594 goat anti-mouse IgG (A-11032; lot 1170050) antibodies were obtained from Life Technologies, Inc. HRP-conjugated goat AffiniPure anti-rabbit IgG (H+L) (111-035-144; lot 123520) and HRP-conjugated goat AffiniPure F(ab′)$_2$ fragment goat anti-mouse IgG, F(ab′)$_2$ fragment-specific (115-036-072; lot 111686) antibodies were obtained from Jackson ImmunoResearch (West Grove, PA).

Animals—Cx50D47A (*No2*, ENU-326) mice (originally identified by Favor (33) by screening for the cataract phenotype following ethylnitrosourea mutagenesis) were maintained as described previously (3). All animal procedures followed the University of Chicago Animal Care and Use Committee guidelines.

Organ Culture—Lenses were dissected from 1-month-old wild type mice and placed in medium 199 without phenol red containing 1 μM thapsigargin, 0.1 mM non-essential amino acids, 10% FBS, 2 mM glutamine, 100 units/ml penicillin G, and 10 μg/ml streptomycin sulfate. After 24 h, lenses were collected and processed for RT-qPCR or immunofluorescence.

Reverse Transcription Real-time PCR—Lenses from 1-month-old mice littermates of different genotype were homogenized in QIAzol Lysis Reagent (Qiagen, Valencia, CA) using a glass-glass homogenizer, and the RNA was purified using the miRNeasy minikit (Qiagen). RNA concentrations were determined using a Nanodrop spectrophotometer (NanoDrop Products, Wilmington, DE), and RNA quality was analyzed on an Agilent Bio-Analyzer (Agilent Technologies, Santa Clara, CA). cDNA was synthesized using the QuantiTect Reverse Transcription Kit (Qiagen). Real-time PCR was performed on a 7500 Fast Real-Time PCR System (Applied Biosystems, Foster City, CA) using a cDNA aliquot, a primer set (as indicated in Table 1), and Fast SYBR® Green Master Mix (Life Technologies, Inc.). Primer sets were accepted for further work if their efficiencies were within a 95% confidence value and they did not produce primer dimers as assessed by the melting curves. All reaction mixes contained equal amounts of RNA. Each sample was run in triplicate for each primer set in any one

TABLE 1
Primers for real-time PCR

Target RNA	Primer sequence
Total *Xbp-1*	
Sense	GAACCAGGAGTTAAGAACACG
Antisense	AGGCAACAGTGTCAGAGTCC
Spliced *Xbp-1*	
Sense	AGCTTTTACGGGAGAAAACTCA
Antisense	GCCTGCACCTGCTGCG
CHOP	
Sense	CTGCCTTTCACCTTGGAGAC
Antisense	CGTTTCCTGGGGATGAGATA
p58^{IPK}	
Sense	TCCTGGTGGACCTGCAGTACG
Antisense	CTGCGAGTAATTTCTTCCCC
Erp72	
Sense	AGTCAAGGTGGTGGTGGGAAAG
Antisense	TGGGAGCAAAATAGATGGTAGGG
Trib3	
Sense	TGGCTGGCAGATACCCATTC
Antisense	CAAGTCGCTCTGAAGGTTCCTT
Irs2	
Sense	GGGGCGAACTCTATGGGTA
Antisense	GCAGGCGTGGTTAGGGAAT
Cyclophilin A	
Sense	TATCTGCACTGCCAAGACTG
Antisense	ACAGTCGGAAATGGTGATCT

of three independent experiments. The transcript for the housekeeping gene, cyclophilin A, was used to normalize the relative levels of RNA among the different genotypes. Graphs were prepared using SigmaPlot version 10.0 (Systat Software, Inc., San Jose, CA).

Immunoblotting—Whole lens homogenates from 1-month-old mice were prepared in PBS (pH 7.4) containing 4 mM EDTA, 2 mM PMSF, and cOmplete EDTA-free protease inhibitor mixture (Roche Applied Science) using a glass-glass homogenizer followed by sonication. Protein concentrations were determined in the total homogenates using the Bio-Rad Protein Assay Dye Reagent Concentrate based on the method of Bradford (34). Immunoblots for antibodies from Cell Signaling Technology were performed following the company's immunoblot protocol. Samples were collected in SDS-containing sample buffer and homogenized using a glass-glass homogenizer. Protein concentrations were determined using the Pierce 660-nm protein assay (Thermo Fisher Scientific). Aliquots from lens homogenates containing equal amounts of total protein were loaded in each lane and resolved on SDS-polyacrylamide gels. Gels were then blotted to Immobilon P membranes (Millipore, Bedford, MA) using a wet transfer apparatus, because we have found that this electroblotting system results in even transfer of the proteins across the lanes. (We confirmed equivalence of loading and transfer by staining of parallel gels with Coomassie Brilliant Blue or of membranes with Ponceau S. The predominant proteins stained in lens homogenates by these methods are crystallins. See supplemental Fig. 1.) Then the membranes were subjected to immunoblotting as described previously (35). The bands obtained in at least three independent experiments were quantified by densitometry using Adobe Photoshop CS3 (Adobe Systems Inc., San Jose, CA). The results are reported as relative values of the levels detected in wild type lenses. Graphs were prepared using SigmaPlot version 10.0 (Systat Software). Data were analyzed for statistical significance using Student's *t* test. A p value of <0.05 was considered significant.

Immunofluorescence—One-month-old lenses were fixed in 4% paraformaldehyde in PBS for 1 h at room temperature. Then they were rinsed three times with PBS, transferred to 30% sucrose in PBS, and left at 4 °C until they sank. Lenses were cryosectioned using an HM 550 M cryostat (Thermo Fisher Scientific), and sections were collected on polylysine-coated slides (PolySciences Inc., Warrington, PA). Then sections were incubated in PBS containing 5% normal goat serum and 0.3% Triton X-100 for 1 h at room temperature, followed by an overnight incubation in primary antibodies diluted in PBS containing 1% BSA and 0.3% Triton X-100 at 4 °C. After several rinses in PBS, sections were incubated in secondary antibodies diluted in PBS containing 1% BSA and 0.3% Triton X-100 for 1.5 h at room temperature. Subsequently, sections were rinsed several times with PBS, incubated with DAPI (Life Technologies) for 15 min at room temperature to stain nuclei, and rinsed with PBS. Coverslips were mounted using 4% *n*-propylgallate in PBS/glycerol (1:4) or ProLong® Gold antifade mountant (Life Technologies). Specimens were observed with an Olympus Plan Apo N ×60 (numerical aperture 1.42) oil immersion objective using an Olympus IX81 (Center Valley, PA) confocal microscope using the laser company settings for Alexa488, Alexa594, and DAPI or with a Zeiss Plan Apochromat ×10 (numerical aperture 0.45) or ×40 (numerical aperture 1.0) objective in an Axioplan 2 microscope (Carl Zeiss Inc.) equipped with a mercury lamp and the appropriate filter sets. Figures were assembled using Adobe Photoshop CS3 (Adobe Systems) and show representative images from at least three independent experiments.

P-PERK immunofluorescence was quantified using results of four independent experiments. Between 4 and 11 confocal images from each genotype were acquired from each experiment. The integrated density (Σ (stained area × mean intensity)) of immunopositive P-PERK particles in each image was quantified using ImageJ (36) after applying a threshold. The threshold was kept constant for all images within an experiment. The results are reported in arbitrary units as the average of the integrated density of all images in each individual experiment and as the overall mean for each genotype. Statistical analysis was performed using paired Student's *t* test. A p value of <0.05 was considered significant.

TUNEL Staining—Cryostat sections from paraformaldehyde-fixed lenses were subjected to TUNEL staining using the Fluorescein *in Situ* Cell Death Detection Kit (Roche Applied Science; 11684795910; lot 11905500), following the manufacturer's instructions after permeabilization of the sections in freshly prepared 0.1% Triton X-100, 0.1% sodium citrate for 5 min on ice. Sections treated with 96 Kunitz units/ml RNase-free DNase I (Qiagen) for 2 min were used as a positive control. Specimens were observed in an Axioplan 2 microscope (Carl Zeiss Inc.) equipped with a mercury lamp. Images were acquired with a Zeiss AxioCam digital camera using Zeiss AxioVision software. Figures were assembled using Adobe Photoshop CS3. The integrated density of TUNEL staining in each image was quantified using ImageJ after applying a threshold. The threshold was kept constant for all images within an exper-

iment. Five independent experiments (analyzing 2–9 images of each genotype) were used to calculate the integrated density. The results are reported as the average of integrated density in each genotype for each experiment and as the overall percentage change for each genotype. Statistical analysis was performed using paired Student's *t* test. A p value of <0.05 was considered significant.

Author Contributions—V. M. B. and E. C. B. conceived and coordinated the study. V. M. B. and E. C. B. wrote the paper with contributions from P. J. M. and P. A. L. P. J. M., P. A. L., and J. I. S. performed the experiments. All authors approved the final version of the manuscript.

References

1. Arora, A., Minogue, P. J., Liu X., Addison, P. K., Russel-Eggitt, I., Webster, A. R., Hunt, D. M., Ebihara, L., Beyer, E. C., Berthoud, V. M., and Moore, A. T. (2008) A novel connexin50 mutation associated with congenital nuclear pulverulent cataracts. *J. Med. Genet.* **45,** 155–160
2. Steele, E. C., Jr., Lyon, M. F., Favor, J., Guillot, P. V., Boyd, Y., and Church, R. L. (1998) A mutation in the connexin 50 (Cx50) gene is a candidate for the *No2* mouse cataract. *Curr. Eye Res.* **17,** 883–889
3. Berthoud, V. M., Minogue, P. J., Yu, H., Schroeder, R., Snabb, J. I., and Beyer, E. C. (2013) Connexin50D47A decreases levels of fiber cell connexins and impairs lens fiber cell differentiation. *Invest. Ophthalmol. Vis. Sci.* **54,** 7614–7622
4. Alge, C. S., Priglinger, S. G., Neubauer, A. S., Kampik, A., Zillig, M., Bloemendal, H., and Welge-Lussen, U. (2002) Retinal pigment epithelium is protected against apoptosis by αB-crystallin. *Invest. Ophthalmol. Vis. Sci.* **43,** 3575–3582
5. Dasgupta, S., Hohman, T. C., and Carper, D. (1992) Hypertonic stress induces αB-crystallin expression. *Exp. Eye Res.* **54,** 461–470
6. de Jong, W. W., Leunissen, J. A. M., and Voorter, C. E. M. (1993) Evolution of the α-crystallin/small heat-shock protein family. *Mol. Biol. Evol.* **10,** 103–126
7. Goldfarb, L. G., Vicart, P., Goebel, H. H., and Dalakas, M. C. (2004) Desmin myopathy. *Brain* **127,** 723–734
8. Ye, J., Rawson, R. B., Komuro, R., Chen, X., Davé, U. P., Prywes, R., Brown, M. S., and Goldstein, J. L. (2000) ER stress induces cleavage of membrane-bound ATF6 by the same proteases that process SREBPs. *Mol. Cell* **6,** 1355–1364
9. Haze, K., Yoshida, H., Yanagi, H., Yura, T., and Mori, K. (1999) Mammalian transcription factor ATF6 is synthesized as a transmembrane protein and activated by proteolysis in response to endoplasmic reticulum stress. *Mol. Biol. Cell* **10,** 3787–3799
10. Bassnett, S., and Mataic, D. (1997) Chromatin degradation in differentiating fiber cells of the eye lens. *J. Cell Biol.* **137,** 37–49
11. Sathyanarayana, P., Dev, A., Fang, J., Houde, E., Bogacheva, O., Bogachev, O., Menon, M., Browne, S., Pradeep, A., Emerson, C., and Wojchowski, D. M. (2008) EPO receptor circuits for primary erythroblast survival. *Blood* **111,** 5390–5399
12. Klooster, R., Eman, M. R., le Duc, Q., Verheesen, P., Verrips, C. T., Roovers, R. C., and Post, J. A. (2009) Selection and characterization of KDEL-specific VHH antibody fragments and their application in the study of ER resident protein expression. *J. Immunol. Methods* **342,** 1–12
13. Ng, C. L., Oresic, K., and Tortorella, D. (2010) TRAM1 is involved in disposal of ER membrane degradation substrates. *Exp. Cell Res.* **316,** 2113–2122
14. Hershey, J. W. B. (1991) Translational control in mammalian cells. *Annu. Rev. Biochem.* **60,** 717–755
15. Lin, J. H., Li, H., Zhang, Y., Ron, D., and Walter, P. (2009) Divergent effects of PERK and IRE1 signaling on cell viability. *PLoS One* **4,** e4170
16. Rashid, H.-O., Yadav, R. K., Kim, H.-R., and Chae, H.-J. (2015) ER stress: autophagy induction, inhibition and selection. *Autophagy* **11,** 1956–1977
17. Acosta-Alvear, D., Zhou, Y., Blais, A., Tsikitis, M., Lents, N. H., Arias, C., Lennon, C. J., Kluger, Y., and Dynlacht, B. D. (2007) XBP1 controls diverse cell type- and condition-specific transcriptional regulatory networks. *Mol. Cell* **27,** 53–66
18. Hamanaka, R. B., Bobrovnikova-Marjon, E., Ji, X., Liebhaber, S. A., and Diehl, J. A. (2009) PERK-dependent regulation of IAP translation during ER stress. *Oncogene* **28,** 910–920
19. Jousse, C., Deval, C., Maurin, A.-C., Parry, L., Chérasse, Y., Chaveroux, C., Lefloch, R., Lenormand, P., Bruhat, A., and Fafournoux, P. (2007) TRB3 inhibits the transcriptional activation of stress-regulated genes by a negative feedback on the ATF4 pathway. *J. Biol. Chem.* **282,** 15851–15861
20. Ohoka, N., Yoshii, S., Hattori, T., Onozaki, K., and Hayashi, H. (2005) *TRB3*, a novel ER stress-inducible gene, is induced via ATF4-CHOP pathway and is involved in cell death. *EMBO J.* **24,** 1243–1255
21. Tanaka, T., Tsujimura, T., Takeda, K., Sugihara, A., Maekawa, A., Terada, N., Yoshida, N., and Akira, S. (1998) Targeted disruption of ATF4 discloses its essential role in the formation of eye lens fibres. *Genes Cells* **3,** 801–810
22. Alapure, B. V., Stull, J. K., Firtina, Z., and Duncan, M. K. (2012) The unfolded protein response is activated in connexin 50 mutant mouse lenses. *Exp. Eye Res.* **102,** 28–37
23. Tattersall, D., Scott, C. A., Gray, C., Zicha, D., and Kelsell, D. P. (2009) EKV mutant connexin 31 associated cell death is mediated by ER stress. *Hum. Mol. Genet.* **18,** 4734–4745
24. Ikesugi, K., Yamamoto, R., Mulhern, M. L., and Shinohara, T. (2006) Role of the unfolded protein response (UPR) in cataract formation. *Exp. Eye Res.* **83,** 508–516
25. Mulhern, M. L., Madson, C. J., Danford, A., Ikesugi, K., Kador, P. F., and Shinohara, T. (2006) The unfolded protein response in lens epithelial cells from galactosemic rat lenses. *Invest. Ophthalmol. Vis. Sci.* **47,** 3951–3959
26. Watson, G. W., and Andley, U. P. (2010) Activation of the unfolded protein response by a cataract-associated αA-crystallin mutation. *Biochem. Biophys. Res. Commun.* **401,** 192–196
27. Xi, J.-H, Bai, F., Gross, J., Townsend, R. R., Menko, A. S., and Andley, U. P. (2008) Mechanism of small heat shock protein function *in vivo*: a knock-in mouse model demonstrates that the R49C mutation in αA-crystallin enhances protein insolubility and cell death. *J. Biol. Chem.* **283,** 5801–5814
28. Horwitz, J. (1992) α-Crystallin can function as a molecular chaperone. *Proc. Natl. Acad. Sci. U.S.A.* **89,** 10449–10453
29. Firtina, Z., and Duncan, M. K. (2011) Unfolded protein response (UPR) is activated during normal lens development. *Gene Expr. Patterns* **11,** 135–143
30. Rong, P., Wang, X., Niesman, I., Wu, Y., Benedetti, L. E., Dunia, I., Levy, E., and Gong, X. (2002) Disruption of *Gja8* (α8 connexin) in mice leads to microphthalmia associated with retardation of lens growth and lens fiber maturation. *Development* **129,** 167–174
31. White, T. W., Goodenough, D. A., and Paul, D. L. (1998) Targeted ablation of connexin50 in mice results in microphthalmia and zonular pulverulent cataracts. *J. Cell Biol.* **143,** 815–825
32. Sellitto, C., Li, L., and White, T. W. (2004) Connexin50 is essential for normal postnatal lens cell proliferation. *Invest. Ophthalmol. Vis. Sci.* **45,** 3196–3202
33. Favor, J. (1983) A comparison of the dominant cataract and recessive specific-locus mutation rates induced by treatment of male mice with ethylnitrosourea. *Mutat. Res.* **110,** 367–382
34. Bradford, M. M. (1976) A rapid and sensitive method for the quantitation of microgram quantities of protein utilizing the principle of protein-dye binding. *Anal. Biochem.* **72,** 248–254
35. Minogue, P. J., Tong, J. J., Arora, A., Russell-Eggitt, I., Hunt, D. M., Moore, A. T., Ebihara, L., Beyer E. C., and Berthoud, V. M. (2009) A mutant connexin50 with enhanced hemichannel function leads to cell death. *Invest. Ophthalmol. Vis. Sci.* **50,** 5837–5845
36. Schneider, C. A., Rasband, W. S., and Eliceiri, K. W. (2012) NIH Image to ImageJ: 25 years of image analysis. *Nat. Methods* **9,** 671–675